Calorimetric System for Measurement of Synchronous Machine Losses

Paavo Rasilo, Jussi Ekström, Ari Haavisto, Anouar Belahcen, Antero Arkkio

Aalto University School of Electrical Engineering, Dept. of Electrical Engineering, P.O. Box 13000 FI-00076 Aalto, Finland

E-mail: paavo.rasilo@aalto.fi

Abstract

An open-cycle air-cooled calorimetric system for the measurement of power losses of a 150-kVA synchronous generator is described. The enthalpy increase and mass flow of the cooling air are determined by measuring the temperature rise, relative humidity, absolute pressure and the pressure drop over a known aerodynamic resistance. The loss measurements are performed using the balance method by calibrating the system against a set of heating resistors. In addition, the difference in heat leakage between the balance test and actual test run is determined by measuring two additional calibration curves. The losses of the test machine are measured in three different loading points. From the error analysis, measurement errors of 5.0 % and 1.9 % are obtained for the total electromagnetic loss at no load and in rated-load operation, respectively.

Nomenclature

Symbols

a, b	constant parameters	RH	relative humidity
c_p	specific heat capacity	T	temperature
C	discharge factor	v	air velocity in tube
d	orifice diameter	x	absolute humidity
D	tube diameter	$x_{1\ldots6}$	measured variables
h	enthalpy	β	diameter ratio
p	pressure	$\Delta\cdot$, $\Delta(\cdot)$	uncertainty of the succeeding quantity (except for h, p, q and Q)
p_0	atmospheric pressure	Δh	enthalpy increase
P	electrical or mechanical power	Δp	pressure difference over orifice plate
q	heat leakage	Δq	leakage difference
q_m	mass flow rate	ΔQ	thermal power increase
Q	thermal power	ε	expansion factor
r	loss distribution in calorimeter	μ	dynamic viscosity
R	specific gas constant	ρ	mass density
Re	Reynold's number		

Subindices

a	dry air	low	(pressure) after orifice plate
b	balance test	out	outlet/output
core	core (loss)	r	rotor
Cu	copper (loss)	res	heating resistors
in	inlet/input	s	stator
em	electromagnetic (loss)	t	test run
fw	friction and windage (loss)	w	water vapor
hi	(pressure) before orifice plate	ws	saturated water vapor
loss	power loss		

1. Introduction

Due to increasing need for energy efficiency, accurate methods are needed to determine the power losses of electrical machines by measurements. Because of high efficiency of electrical machinery, the most commonly used and easily implemented input-output method [1] can lead to unacceptably inaccurate results when losses in loaded conditions are studied. For better accuracy, calorimetry [2] can be used.

The calorimetric method is used to determine the losses directly from the heat dissipation of the machine. During the past twenty years, the calorimetric method has been used quite widely to determine the losses and efficiency of electrical machinery, mostly induction machines [3]-[13]. Different implementations from closed-cycle water-cooled systems [3], [4] to high-precision calorimeters with seemingly complex arrangements [5]-[7] have been reported. However, with balanced calorimeters calibrated with a known heat source, accurate results can be obtained even with relatively simple constructions and open-cycle cooling with air as the coolant fluid [8], [9].

In this paper, a balance calorimeter is designed for a 150-kVA synchronous generator. The aim is to obtain good measurement accuracy for the total electromagnetic loss in different loading conditions and also with frequency-converter supply. By measuring the armature resistance and excitation power, the total electromagnetic losses are further segregated into stator and rotor winding copper losses and core losses. In addition to iron loss, the core loss comprises also other loss components which are included in the total electromagnetic loss but not in the copper losses calculated using the DC resistances of the windings.

Since the studied machine is air cooled, the open-cycle air-cooled construction was chosen for the calorimeter. The heat capacity and mass-flow rate of the coolant air are determined accurately during the measurements. This eliminates the need for the balance test following each test run, after the system is once calibrated. In the calibration, the possibility of determining the short-circuit losses of the synchronous generator from the shaft power is exploited. Comparison of the short-circuit tests and the balance tests allows to evaluate dependency of the heat leakage on the physical location of the heat source inside the calorimeter.

As an application, the electromagnetic losses of the test machine are measured in no-load operation and with two different loads in the motoring mode of operation with supply from the grid. When the loading increases from no load to the rated load, the measurement error decreases from 5.0 % to 1.9 %. Similar accuracy is expected also for a machine supplied from a frequency converter.

2. Principle of the Balance Calorimeter

In the calorimetric method, the test machine is insulated from its environment in such way that all of the losses to be measured are transformed as heat to the cooling circuits of the system [2]. When the properties of the coolant flowing in these cooling circuits are measurable, the losses can be determined as the rate of change of the coolant's thermal energy.

Fig. 1 presents the power flow of the calorimetric system. P stands for electrical or mechanical power, Q for thermal power and q for heat leakage out from the calorimeter. The following equations are obtained for the steady thermal state:

$$P_{\text{in}} = P_{\text{out}} + P_{\text{loss}}\,, \tag{1}$$

$$Q_{\text{in}} + P_{\text{loss}} = Q_{\text{out}} + q\,. \tag{2}$$

In case of the wound-field synchronous machine under consideration, the power loss P_{loss} consists of the friction and windage loss P_{fw}, stator copper loss $P_{\text{Cu,s}}$, rotor copper loss $P_{\text{Cu,r}}$ and the core loss P_{core}. The last three together form the electromagnetic losses P_{em}:

$$P_{\text{loss}} = P_{\text{fw}} + P_{\text{Cu,s}} + P_{\text{Cu,r}} + P_{\text{core}} = P_{\text{fw}} + P_{\text{em}}\,. \tag{3}$$

In case of a balance calorimeter, the system is calibrated with heating resistors providing a known heat source. The idea is that

the heat flow of the actual machine test (subindex t) is compared to the heat flow of the balance test (b) in which power is supplied to the resistors:

$$P_{\mathrm{in,t}} - P_{\mathrm{out,t}} = \left(Q_{\mathrm{out,t}} - Q_{\mathrm{in,t}}\right) + q_{\mathrm{t}} \tag{4}$$

$$P_{\mathrm{in,b}} = \left(Q_{\mathrm{out,b}} - Q_{\mathrm{in,b}}\right) + q_{\mathrm{b}}. \tag{5}$$

If both the thermal power increase and leakage remain unchanged between the two tests ($Q_{\mathrm{out,t}} - Q_{\mathrm{in,t}} = Q_{\mathrm{out,b}} - Q_{\mathrm{in,b}}$ and $q_{\mathrm{t}} = q_{\mathrm{b}}$), the input power of the balance test equals the loss of the machine:

$$P_{\mathrm{in,b}} = P_{\mathrm{in,t}} - P_{\mathrm{out,t}} = P_{\mathrm{loss}} = P_{\mathrm{fw}} + P_{\mathrm{em}} . \tag{6}$$

During the balance test, the synchronous machine is rotated by a prime mover to ensure that the cooling conditions inside the calorimeter are identical to those during the actual test run. Thus the total input power in the balance test consists of the power P_{res} supplied to the resistors and the friction and windage loss P_{fw} supplied by the prime mover:

$$P_{\mathrm{in,b}} = P_{\mathrm{res}} + P_{\mathrm{fw}} . \tag{7}$$

This means that after identical thermal conditions have been reached, the power supplied to the resistors is equal to the electromagnetic loss of the machine:

$$P_{\mathrm{res}} = P_{\mathrm{em}} = P_{\mathrm{Cu,s}} + P_{\mathrm{Cu,r}} + P_{\mathrm{core}} . \tag{8}$$

To ensure that the thermal conditions remain unchanged between the test run and the balance test, the thermal power increase of the coolant air flowing through the calorimeter has to be measured. The increase is obtained from the mass-flow rate q_{m} and the increase Δh in the coolant's enthalpy:

$$\Delta Q = Q_{\mathrm{out}} - Q_{\mathrm{in}} = q_{\mathrm{m}} \Delta h . \tag{9}$$

Measurement of these quantities is described in Section 4.

Before the final value for the thermal power increase can be determined, the system must have reached a steady thermal state in which the temperatures and losses have stabilized. Standard [2] considers the steady state to have been reached when the variation in the losses is less than 1 % over a period of two hours or when the variation in the coolant's temperature rise is less than 1 % in one hour. In this work, both requirements are considered simultaneously, the first one applied to the thermal power increase (9). All the measurements described later in this paper are performed by recording the values at roughly 10-s intervals and averaging the values over the last 20 minutes of measurement.

3. Design of the Calorimetric System

3.1. Test Machine

The test machine is a 4-pole 150-kVA, 400-V, 50/60-Hz synchronous generator with rated displacement factor of 0.8 capacitive. Designed for a diesel-generator application, the machine is originally of single-bearing construction, and thus an additional supporting bearing was mounted to the drive end (D-end) to allow accurate coupling to an induction motor for driving and loading purposes.

The cooling of the machine is of open-cycle asymmetric type, the cooling air flowing from the non-drive end (N-end) to the D-end through the air gap and between the stator core and the frame. The air flow is ensured by a shaft-mounted fan in the D-end. The maximum power losses of the machine were estimated to be 12 kW or 10 % of the rated active power.

3.2. Calorimeter Construction

The simplest choice for the calorimeter construction is the open-cycle air-cooled type in which the machine is cooled with the air taken from the calorimeter inlet and removed from the outlet. The required coolant flow was estimated to be around 0.2 m^3/s, which would result in a cooling air temperature rise of around 60 °C.

Simplified view of the calorimeter is shown in Fig. 2. 50-mm Finnfoam® compressed polystyrene sheets were chosen as the construction material of the walls and the ceiling of the calorimeter. The walls were attached to a planed-board frame while a 30-mm plywood sheet was used as the base. Under the plywood, a 70-mm Finnfoam sheet was placed, except under the fixing supports of the machine, where pieces of glued laminated beam were used to obtain a good mechanical strength against the forces transferred to the base. In the mounting of the machine, metal-to-metal contacts were avoided by placing thin pieces of plywood between the machine support and the fixing block (Fig. 3 a)).

The whole inner surface of the calorimeter was coated with 1-mm aluminum sheets to reflect radiating heat and to balance the temperature distribution over the surface of the walls. To reduce heat leakage, the shaft hole through the calorimeter wall was insulated from the outside by two 9-mm cellular rubber sheets punched with a hole just equal to the shaft diameter. The test machine was coupled to the induction machine using a jaw coupling, which was left outside the calorimeter, but separately surrounded by Finnfoam sheets to reduce convective heat transfer to the room. The two shafts were thermally isolated from each other by the plastic hub of the coupling (Fig. 3 b)).

The system was placed in a 1600-m^3 test hall capable of maintaining supply and exhaust air flow rates of 4300 m^3/h. Round 200-mm ventilation tube was used as the inlet and outlet of the calorimeter, the inlet air taken directly from the room. The outgoing air from the calorimeter was taken outside of the room by a separate exhaust fan. Between the calorimeter outlet and the exhaust fan, a tube with an orifice plate was installed for the air flow-rate measurement. From the outlet to the orifice plate, the exhaust tube was insulated with a 100-mm thick rock-wool pipe insulation to prevent the air from cooling before the orifice plate.

3.3. Power Supply

An isolated 400-V, 50-Hz grid was created with a synchronous generator run by a grid-connected synchronous motor. Automatic excitation control was able to maintain steady voltage in the isolated grid.

A four-quadrant frequency converter supplying the load/prime-mover induction machine was connected to the same grid. The power supply was designed so that the grid and the frequency-converter supplies can easily be interchanged to study the additional inverter losses in the test machine. In this paper, however, only the sinusoidal supply is considered.

The excitation for the test machine was supplied through a variable three-phase transformer, a diode-bridge rectifier and a pair of slip rings mounted in the N-end. The power to the three parallel-connected 20-Ω heating resistors was supplied by coupling a DC generator to a grid-supplied induction machine allowing the power to be controlled through the generator excitation. Despite the temperature rise during the tests, manual control was found sufficient both for the heating-resistor and the field-winding supplies.

4. Methods of Measurement and Calculation

4.1. Measurement of Enthalpy Increase

If the coolant air is treated as an ideal gas, the increase in its enthalpy (per unit mass of humid air) when flowing through the calorimeter can be defined as

$$\Delta h\left(T_{\text{in}},T_{\text{out}},x\right)=\frac{\int_{T_{\text{in}}}^{T_{\text{out}}}\left[c_{p,\text{a}}\left(T\right)+xc_{p,\text{w}}\left(T\right)\right]dT}{1+x}, \tag{10}$$

where T_{in} and T_{out} are the inlet and outlet temperatures, $c_{p,\text{a}}(T)$ and $c_{p,\text{w}}(T)$ are the specific heat capacities of dry air and water vapor, respectively, and x is the absolute humidity which is assumed to be constant throughout the cooling cycle [14]. Since the temperature dependency of the specific heats is not very significant on the presented application's practical temperature range T = 20…100 °C, average values over the inlet and outlet temperatures may be used to avoid the integration.

To take into account possible variations in the temperature distribution over the cross-sections of the inlet and outlet tubes, the temperatures of the coolant air were averaged over three four-wire Pt-100 temperature sensors placed in the center and in the edges of the tubes. To determine the absolute humidity, a relative humidity sensor was installed in the inlet tube of the coolant air. When the relative humidity RH_{in} is measured and the saturation vapor pressure $p_{\text{ws}}(T_{\text{in}})$ for the current temperature T_{in} is known, the pressure of the water vapor is obtained from

$$p_{\text{w,in}}=RH_{\text{in}}p_{\text{ws}}\left(T_{\text{in}}\right). \tag{11}$$

The temperature dependency of the saturation pressure can be approximated e.g. as

$$p_{\text{ws}}\left(T_{\text{in}}\right)=\frac{e^{77.345+0.0057\frac{T_{\text{in}}}{\text{K}}-7235\frac{\text{K}}{T_{\text{in}}}}}{\left(T_{\text{in}}/\text{K}\right)^{8.2}}\ \text{Pa}, \tag{12}$$

where T_{in} is expressed in the Kelvin scale. The commonly used equation has been obtained by curve fitting to experimental data of [15]. After the water vapor pressure is obtained, its density can be calculated from the ideal gas law as

$$\rho_{\text{w,in}}=\frac{p_{\text{w,in}}}{T_{\text{in}}R_{\text{w}}}, \tag{13}$$

where R_{w} is the specific gas constant of water vapor.

The barometric air pressure p_0 was measured with an absolute pressure transducer. According to Dalton's law of partial pressures, the density of dry air in the inlet is

$$\rho_{\text{a,in}}=\frac{p_{\text{a,in}}}{T_{\text{in}}R_{\text{a}}}=\frac{p_0-p_{\text{w,in}}}{T_{\text{in}}R_{\text{a}}}. \tag{14}$$

The absolute humidity needed for the calculation of the specific heat is now obtained as the mass-density ratio of water vapor and air:

$$x=\frac{\rho_{\text{w,in}}}{\rho_{\text{a,in}}}. \tag{15}$$

4.2. Air Flow-Rate Measurement

The flow-rate measurement for the coolant air was performed according to standard [16], [17] by measuring the pressure drop over a calibrated orifice plate. The outlet air was run through a long tube with a diameter of D = 96 mm, in the middle of which the orifice plate with a bore of d = 72 mm was mounted. The pressure drop Δp over the orifice plate was measured using both an electric differential pressure transducer and a water manometer. The absolute pressures p_{hi} and p_{low} on both sides of the orifice were also measured by electric absolute pressure transducers. The mass density of the incoming air at temperature T_{out} was determined from the partial densities as

$$\rho = \rho_{\mathrm{a}} + \rho_{\mathrm{w}} \tag{16}$$

using (11)-(14).

The mass flow rate was calculated according to [16] as

$$q_{\mathrm{m}} = \frac{\varepsilon C}{\sqrt{1-\beta^4}} \left(\frac{\pi}{4} d^2 \right) \sqrt{2\rho\Delta p}\,, \tag{17}$$

in which the following quantities are used:

diameter ratio $$\beta = \frac{d}{D}\,, \tag{18}$$

velocity of approach factor $$\frac{1}{\sqrt{1-\beta^4}}\,, \tag{19}$$

expansion factor $$\varepsilon = \varepsilon\left(\beta, \frac{p_{\mathrm{low}}}{p_{\mathrm{hi}}} \right) \tag{20}$$

and discharge factor $$C = C\left(\beta, Re\right). \tag{21}$$

The expansion factor and discharge factor were determined according to [17]. The expansion factor takes into account the compressibility of air and depends on the diameter ratio and the relative pressure difference over the orifice. The discharge factor depends on the diameter ratio and the Reynold's number Re, which is defined as

$$Re = \frac{D\rho v}{\mu\left(x, T_{\mathrm{out}}\right)}, \tag{22}$$

where v is the air velocity in the tube and $\mu(x,T_{\mathrm{out}})$ is the dynamic viscosity of the coolant at the current temperature. The dynamic viscosity of humid air can be calculated according to [18].

Since the air speed

$$v = \frac{q_{\mathrm{m}} / \rho}{\frac{\pi}{4} D^2} \tag{23}$$

and thus also the Reynold's number depend on the flow rate itself, solution of (17) together with (18)-(23) requires an iterative procedure. The solution was obtained by initializing the Reynold's number to 10^5 and then solving (21), (17), (23) and (22) in successive order until convergence was reached. Two or three iterations were found to be enough in most cases.

4.3. Other Measurements

The test machine terminal power and the DC powers supplied to the field winding and calibrating resistors were measured with a 12-channel LEM Norma D 6000 power analyzer. The rotor copper losses were directly obtained from the field-winding power.

To determine the copper losses in the armature winding, a cooling curve was determined by measuring the resistance as a function of time during the first couple of minutes after the test machine had been stopped. The resistance at the switch-off instant was determined by extrapolation assuming an exponential form of the cooling curve.

During the calibration tests with loss powers ranging from 1 to 13 kW, the machine torque was measured by a 200-Nm torque transducer calibrated to give an error of less than 1 % on the range of 6…80 Nm. The methods of measurement are summarized in Table I.

5. Accuracy Considerations and Calibration

5.1. Error Analysis

The requirement for the balance calorimeter method to work is that the thermal power increase and leakage during the machine run are equal to those during the balance test. Since the thermal power is calculated based on the enthalpy and mass flow, the major sources of error in the measurement system are:

1. Inaccuracy in the mass-flow measurement
2. Inaccuracy in the enthalpy measurement
3. Difference in leakage between the machine run and balance test.

Measurement errors for the six independent variables $x_{1\ldots6} = \{\Delta p, p_{\mathrm{hi}}, p_0, T_{\mathrm{in}}, T_{\mathrm{out}}, RH_{\mathrm{in}}\}$ used in the mass-flow and enthalpy calculations are shown in Table I. The combined standard uncertainty for the mass flow of (17) is

$$\Delta q_{\mathrm{m}} = \sqrt{\sum_{i=1}^{6}\left(\frac{\partial q_{\mathrm{m}}}{\partial x_i}\Delta x_i\right)^2}\ . \tag{24}$$

The uncertainty $\Delta(\Delta h)$ for the enthalpy increase (10) can be similarly calculated from the last four variables $x_{3\ldots6}$.

Once Δq_{m} and $\Delta(\Delta h)$ are derived into a simpler form by substitution of (10)-(23), the measurement uncertainty can be calculated online during the measurement. As an example, the uncertainties were calculated with inlet temperature of T_{in} = 20 °C and the outlet temperature and the relative humidity varying in the ranges of T_{out} = 30…90 °C and RH_{in} = 0…100 %. For practical reasons, the exhaust fan is run at a constant speed during the measurements and the volume flow of the coolant air is approximately constant. Thus the flow rate was set to a value of 0.25 m^3/s and the corresponding mass flows and pressure differences for different temperatures and humidities were calculated using (11)-(23). The atmospheric pressure and the incoming air pressure near the orifice plate were kept constant at p_0 = 1.013 bar and p_{hi} = 0.99 bar, respectively. For the coolant power increase, the following uncertainties were obtained:

$$\Delta(\Delta Q) \approx \pm 3.2\ \%\ \text{at}\ T_{\mathrm{out}} = 30\ ^{\circ}\mathrm{C}\ \text{and}$$
$$\Delta(\Delta Q) \approx \pm 1.7\ \%\ \text{at}\ T_{\mathrm{out}} = 90\ ^{\circ}\mathrm{C}.$$

Humidity was found to have a negligible effect on the relative uncertainty.

The presented study implies that between the test run and the balance test, the coolant power increase can be kept unchangeable with an error of less than 3.2 %. Due to the absolute inaccuracy in the temperature measurement, the accuracy of the measurement is better with higher temperature rise. This means that the measurement accuracy also improves when the load increases. For safety reasons, the maximum allowable temperature can be set to 90 °C. Ideally the temperature rise could be adjusted as a function of the losses by controlling the mass flow. However, with lower flow rates, the inaccuracy in the mass-flow measurement becomes more significant.

In the previous analysis, the inaccuracies of the Fluke 8842A and Fluke Hydra 2625A + 2620A meters were neglected. The

pressure and humidity transducers give voltage signals as outputs, the measurement of which is much more accurate than the sensors themselves. Also in case of the Pt-100 sensors, the inaccuracy of the sensor overcomes the inaccuracy of the resistance measurement.

The third source of error is the difference in the leakage conditions between the test run and the balance test. The error arises from the fact that during the balance test, the heat source in the calorimeter is physically in a different location than during the test run. A method to determine the difference is described after the initial calibration measurements have been presented.

5.2. Calibration Measurements

Since the setup was built to perform dozens of measurements for a single test machine, it was seen necessary to calibrate the system beforehand to remove the need of performing the balance test after each test run. The thermal power increase ΔQ was measured as a function of the power P_{res} supplied to the heating resistors. As mentioned in Section 2, the test machine was rotated during the calibration to get direct correspondence between the thermal power and the electromagnetic losses. By least-squares fitting, a linear relationship was found:

$$P_{\mathrm{res}} = a_{\mathrm{b}}\Delta Q + b_{\mathrm{b}}, \text{ with } \begin{cases} a_{\mathrm{b}} \approx 1.031 \\ b_{\mathrm{b}} \approx -971 \text{ W}. \end{cases} \tag{25}$$

The measured points and the fitted line are shown in Fig. 4. The difference between the thermal power increase and the resistor power is caused by the friction and windage losses and the heat leakage out from the calorimeter.

The time to reach the steady state during the calibration measurements varied between 4 and 8 hours increasing with the resistor power. If the balance test was to be performed separately after each test run, the total measurement time for one operating point could easily exceed 12 hours. It is likely that the temperature, pressure and humidity of the inlet air will vary during this period of time. Thus a separate balance test following each test run would not bring much additional advantage considering the measurement accuracy, and using the premeasured calibration curves is justified. It is still emphasized that if different machines are to be studied, the calibration curves have to be measured separately for each test machine.

5.3. Determination of Leakage Difference

Provided that the leakage conditions are equal between the test run and the balance test, the electromagnetic losses can be obtained from (25). As mentioned, however, the leakage conditions during the balance test may differ from the ones during the test run due to different physical location of the heat source inside the calorimeter. In the following, an estimate for this leakage difference is determined.

First, the distribution of the losses inside the calorimeter is defined as the ratio between the heater-resistor losses P_{res} and the total loss P_{tot}:

$$r = \frac{P_{\mathrm{res}}}{P_{\mathrm{tot}}} = \frac{P_{\mathrm{res}}}{P_{\mathrm{res}} + P_{\mathrm{loss}}} \in [0,1], \tag{26}$$

where P_{loss} equals the losses in the test machine. The value or r during the calibration measurements of the previous section varies as a function of the resistor power, $r = r_{\mathrm{b}}(P_{\mathrm{res}})$, and is not known exactly since the friction and windage losses were not measured. Thus two additional calibration curves were determined by measuring the total loss power as the sum of the shaft power and the field-winding power both in short-circuit operation and when supplying the heater resistors from the test machine. The first case corresponds to $r = 0$ while in the second case the loss distribution again depends on the resistor power: $r = r_{\mathrm{res}}(P_{\mathrm{res}})$. Fig. 5 shows the measured dependency of the thermal power increase on the total loss power and the value of r in the two cases. By least-squares fitting, the following bilinear relationship between the thermal power increase and the total loss power is obtained:

$$P_{\mathrm{tot}} = P_{\mathrm{res}} + P_{\mathrm{loss}} = \big(a_0 + r\big(a_1 - a_0\big)\big)\Delta Q \text{ with } \begin{cases} a_0 \approx 1.051 \\ a_1 \approx 1.020. \end{cases} \tag{27}$$

The slopes a_0 and a_1 correspond to the values of $r = 0$ and $r = 1$, respectively.

Due to the electromagnetic losses present in the test machine when supplying the heater resistors, a larger proportion of the total losses occur in the test machine than during the original calibration measurements, i.e. $r_{\mathrm{res}} < r_{\mathrm{b}} < 1$. Thus for the worst-case error estimate we can define the loss distribution and its error during the balance test as

$$r_{\mathrm{b}} = \frac{1 + r_{\mathrm{res}}}{2} \tag{28}$$

$$\Delta r_{\mathrm{b}} = \frac{1 - r_{\mathrm{res}}}{2}. \tag{29}$$

The estimated r_{b} and the error limits are also shown in Fig. 5. The uncertainty of r_{res} caused by the errors in the torque, field-winding power and heater-resistor power measurements is assumed to be covered by this worst-case error estimate for r_{b}.

Since the leakage conditions of the short-circuit test correspond to those during the actual test run, the leakage difference Δq between the test run and the original calibration measurements, as also the corresponding error $\Delta(\Delta q)$, can now be defined by applying (27) for $r = 0$ and $r = r_{\mathrm{b}}$:

$$\Delta q = q_0 - q_{\mathrm{b}} = a_0 \Delta Q - \big(a_0 + r_{\mathrm{b}}\big(a_1 - a_0\big)\big)\Delta Q = r_{\mathrm{b}}\big(a_0 - a_1\big)\Delta Q\,, \tag{30}$$

$$\Delta\big(\Delta q\big) = \big(a_0 - a_1\big)\sqrt{\big(r_{\mathrm{b}}\Delta\big(\Delta Q\big)\big)^2 + \big(\Delta Q \Delta r_{\mathrm{b}}\big)^2}\,. \tag{31}$$

Adding the leakage difference to (25) gives the final equation from which the electromagnetic loss during the test run can be determined:

$$P_{\mathrm{em}} = a_{\mathrm{b}}\Delta Q + b_{\mathrm{b}} + \Delta q \tag{32}$$

5.4. Accuracy of the Electromagnetic Losses

The absolute inaccuracy in the total electromagnetic loss of the machine is

$$\Delta P_{\mathrm{em}} = \sqrt{\big(a_{\mathrm{b}}\Delta\big(\Delta Q\big)\big)^2 + \big(\Delta\big(\Delta q\big)\big)^2}\,. \tag{33}$$

Due to the constant term b_{b} in (32), the relative inaccuracy in the electromagnetic loss becomes slightly higher than in the thermal power.

Derived from the values of the current shunts and the user manual of the LEM Norma D 6000 power analyzer [19], the accuracies of the stator current and the field power measurements on the ranges of normal operation are ±0.24…0.29 % and ±0.31 %, respectively. Neglecting any other sources of error, the accuracy of the resistance measurement for the cooling curve is similarly determined from the current shunt accuracy and the data found in the Fluke 8842A user manual [20]. Depending on the temperature, the armature resistance was found to vary in the range of 25...45 mΩ, and the error in this range was ±0.42 %. Combining the errors of the armature current and resistance, the error for the stator copper losses was found to vary in the range of ±0.64…0.71 %. After the errors of the copper losses are known, the error for the core loss is obtained as

$$\Delta P_{\mathrm{core}} = \sqrt{\Delta P_{\mathrm{em}}^2 + \Delta P_{\mathrm{Cu,s}}^2 + \Delta P_{\mathrm{Cu,r}}^2}\,. \tag{34}$$

Since the accuracy of the copper-loss measurements is much better than that of the total electromagnetic loss, the absolute

inaccuracies ΔP_{core} and ΔP_{em} are likely to be close to each other. However, the relative error in the core loss will be greater than in the total electromagnetic loss due to subtraction of the copper losses.

5.5. Accuracy of the Operating Conditions

Usually the losses are to be studied in a predefined operating point and thus it is important to know how accurately the operating point can be maintained and measured. Since the test machine was originally designed to operate as a generator, the operating point is here defined by the line-to-line terminal voltage, apparent terminal power and displacement factor. As a measure of stability of the operation point, the relative standard error (RSE), i.e. the standard deviation divided by the average value, over the 20-min averaging period is calculated for these three quantities. The corresponding measurement errors are calculated according to the LEM Norma D 6000 user manual [19]. In addition, the total harmonic distortion (THD) level in the terminal voltage is considered.

6. Results and Discussion

The losses of the synchronous machine were studied in no-load operation, at 50 % of the rated load and at the rated load. In the no-load operation the machine was rotated with the induction machine and the stator terminals were open. In the loaded cases, the test machine was used as a motor with the rated displacement factor 0.8 capacitive, i.e. supplying reactive power to the grid. The time required to reach the steady state was approximately 6 hours at no load and 8 hours at the rated load. In all the operating points, both the 1 % / 2 h criterion for the thermal power increase and the 1 % / 1 h criterion for the temperature rise were fulfilled.

During the last 20 minutes of measurement, the rated-load operating point was maintained at 400.2 V, 149.55 kVA and 0.806 cap with RSE values of 0.01 %, 0.34 % and 0.16 %, respectively. The corresponding measurement errors were 0.05 %, 0.34 % and 0.39 %. The THD contents in the line-to-line voltage was measured to be 1.1 % at the rated load, which is only slightly increased from the value of 0.9 % observed in the grid voltage when the machines were not running.

The obtained thermal power increase, the total electromagnetic losses obtained from (32) and segregation of the losses are presented in Table II. When the load is increased from the no-load operation to the rated load, the core loss increases by 90 %. This increase is caused by load-dependent core-loss components such as the circulating currents in the parallel paths of the stator winding and the currents flowing through the iron between the damper-winding bars. The iron losses are also increased from the no-load operation due to the overexcited state of the machine. As expected, the absolute inaccuracies in the electromagnetic losses and in the core losses are close to each other. At higher loads the relative inaccuracy in the core loss suffers from the fact that the copper losses grow drastically.

For comparison, the losses were also measured with the input-output method utilizing a 2-kNm torque transducer for the shaft-power measurement. Table II shows the thermal power increase $P_{\text{in-out}} / a_0$ calculated by dividing the total loss from the input-output method by the fitting coefficient obtained at the short-circuit operation. Considering the error limits, these values correspond to the measured thermal power increase. In the input-output method, the inaccuracy for the torque measurement was 2 Nm, i.e. 0.1 % of the full-scale range of the transducer. This significantly increases the relative error with smaller torques. If the input-output method was to be used to study the losses in different loading conditions, smaller torque transducers should be used at smaller loads to guarantee good accuracy. This would complicate the measurement arrangements and increase the costs. Another problem in the input-output method is that measurement of the terminal power becomes much more inaccurate if the machine is supplied from a frequency converter. For accurate results, the machine should be in steady thermal state also if the input-output method is used and thus the required measurement times for a single operating point are likely to be equal in the two methods if the calorimetric system has been calibrated in advance. As mentioned, however, the calibration measurements should be performed again if the test machine is changed.

The accuracy of the system is mostly determined by the temperature and pressure measurements and can thus be easily improved by replacing the sensors with more accurate ones. To optimize the accuracy, the mass-flow control could be improved. For each operating point, it might be possible to find a specific mass flow at which the total error resulting from the inaccuracies in the temperature-rise and the differential-pressure measurements is at its minimum.

The exhaust fan was originally estimated to be capable of maintaining higher air flow than the fan of the test machine, the flow rate of which was estimated to be around 0.2 m^3/s. However during rated-load operation, the temperature of the inlet air taken by the test machine rose up to 42 °C. This implies that more air is going through the test machine than is removed by the exhaust fan and thus the air circulation inside the calorimeter is enhanced. If the leakage is considered, the enhanced circulation is an advantage since it decreases the differences in the temperature distributions between the test run and the calibration measurements. On the other hand, it caused the ambient temperature of the test machine to exceed its rated value. This could, however, be allowed for testing purposes since the local temperatures of the stator end windings and the average temperature of the rotor winding were monitored to keep them in safe operating limits. The coolant flow of the test machine was probably better than estimated by the manufacturer due to the removal of the original brushless exciter machine in the N-end.

7. Conclusion

An open-cycle balance calorimeter for the purpose of measuring electromagnetic losses of a synchronous machine was presented. In addition to calibrating the system with heater resistors, the leakage differences between the test run and the balance test were determined. From the error analysis it is concluded that despite its relatively simple construction and implementation, the system is able to give a good accuracy from no-load to rated-load operation. From the total electromagnetic loss, the core loss can be segregated preserving the same absolute measurement error.

References

[1] International Electrotechnical Commission, "Methods for determining losses and efficiency of rotating electrical machinery from tests (excluding machines for traction vehicles)," *IEC 60034-2*, Genève, Switzerland, 1972.

[2] International Electrotechnical Commission, "Methods for determining losses and efficiency of rotating electrical machinery from tests (excluding machines for traction vehicles) Measurement of losses by the calorimetric method," *IEC 60034-2A*, Genève, Switzerland, 1974.

[3] Lindström, J., "Calorimetric methods for loss measurements of small cage induction motors," Master's Thesis, Helsinki University of Technology, 1994.

[4] Szabados, B, Mihalcea, A., "Design and Implementation of a Calorimetric Measurement Facility for Determining Losses in Electrical Machines," *IEEE Trans. Instrum. Meas.*, Vol. 51., No. 5, pp. 902-907, October 2002

[5] McLeod, P., Bradley, K. J., Ferrah, A., Magill, R., Clare, J. C., Wheeler, P., Sewell, P., "High Precision Calorimetry for the Measurement of Efficiency of Induction Motors," *The 1998 IEEE Industry Applications Conference. Thirty-Third IAS Annual Meeting*, St. Louis, MO, USA, Conf. Publ. Vol. 1, pp. 304-311, October 1998.

[6] Cao, W., Bradley, K. J., Ferrah, A., "Development of a High-Precision Calorimeter for Measuring Power Loss in Electrical Machines," *IEEE Trans. Instrum. Meas.*, Vol. 58, No. 3, pp. 570-577, March 2009

[7] Cao, W., Huang, X., Fench, I., "Design of a 300-kW Calorimeter for Electrical Motor Loss Measurement," *IEEE Trans. Instrum. Meas.*, Vol. 58. No. 7, pp. 2365-2367, July 2009.

[8] Binns, K. J., Turner, D. R., Warne, D. F., Shamsadeen, B. N., "A balanced calorimeter for measurement of induction motor losses," *Fifth International Conference on Electrical Machines and Drives*, London, United Kingdom, Conf. Publ. No. 341, pp. 67-71, September 1991.

[9] Turner, D. R., Binns, K. J., Shamsadeen, B. N., Warne, D. F., "Accurate measurement of induction motor losses using balance calorimeter," *IEE Proc. B*, Vol. 138, No. 5, pp. 233-242, September 1991.

[10] Bowman, J. K., Cascio, R. F., Sayani, M. P., Wilson, T. G., "A Calorimetric Method for Measurement of Total Loss in a Power Transformer," *PESC '91 Record. 22nd Annual IEEE Power Electronics Specialists Conference*, pp. 633-640, June 1991.

[11] Cao, W., Bradley, K. J., "Evaluation of Stray Load Loss in Induction Motors, A Comparison of Input-Output and Calorimetric Methods," *Conference Record of the 2001 IEEE Industry Applications Conference: Thirty-Sixth IAS Annual Meeting*, Vol. 2, pp. 754-761, September/October 2001.

[12] Bradley, K. J., Cao, W, Arellano-Padilla, J., "Evaluation of Stray Load Loss in Induction Motors With a Comparison of Input-Output and Calorimetric Methods," *IEEE Trans. Energy Convers.*, Vol. 21, No. 3, pp. 682-689, September 2006.

[13] Cao, W., Bradley, K. J., Clare, J. C., Wheeler, P. W., "Comparison of Stray Load and Inverter-Induced Harmonic Losses in Induction Motors Using Calorimetric and Harmonic Injection Methods," *IEEE Trans. Ind. Appl.*, Vol. 46, No.1, pp. 249-255, January/Febryary 2010.

[14] Moran, M. J., Shapiro, H. N., Boettner, D. D., Bailey, M. B., "Fundamentals of Engineering Themodynamics," 7th edition, John Wiley & Sons, Inc., USA, 2010.

[15] Landoldt, H., Börnstein, R., "Zahlenwerte und Functionen aus Physik-Chemie-Astronomie-Geophysik-Technik," Springer-Verlag, Berlin, Germany, 1960.

[16] European Committee for Standardization, "Measurement of fluid flow by means of pressure differential devices inserted in circular cross-section conduits running full – Part 1: General principles and requirements," *EN ISO 5176-1*, Brussels, Belgium, 2003.

[17] European Committee for Standardization, "Measurement of fluid flow by means of pressure differential devices inserted in circular cross-section conduits running full – Part 2: Orifice plates," *EN ISO 5176-2*, Brussels, Belgium, 2003.

[18] Tsilingiris, P. T., "Thermophysical and transport properties of humid air at temperature range between 0 and 100 °C," *Energy Conversion and Management*, Vol. 49, pp. 1098-1110, November 2007.

[19] LEM Norma GmbH, "Wide Band Power Analyzer D 6000 Operating Instructions," Edition 5E, Wiener Neudorf, Austria, 1996.

[20] John Fluke Mfg. Co., Inc., "8842A Digital Multimeter Instruction Manual," Everett, WA, USA, 1991.

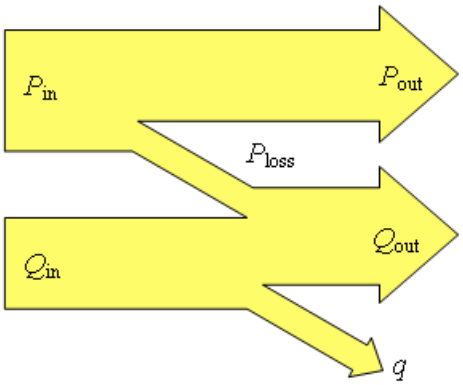

Fig. 1 Power flow of the calorimetric system.

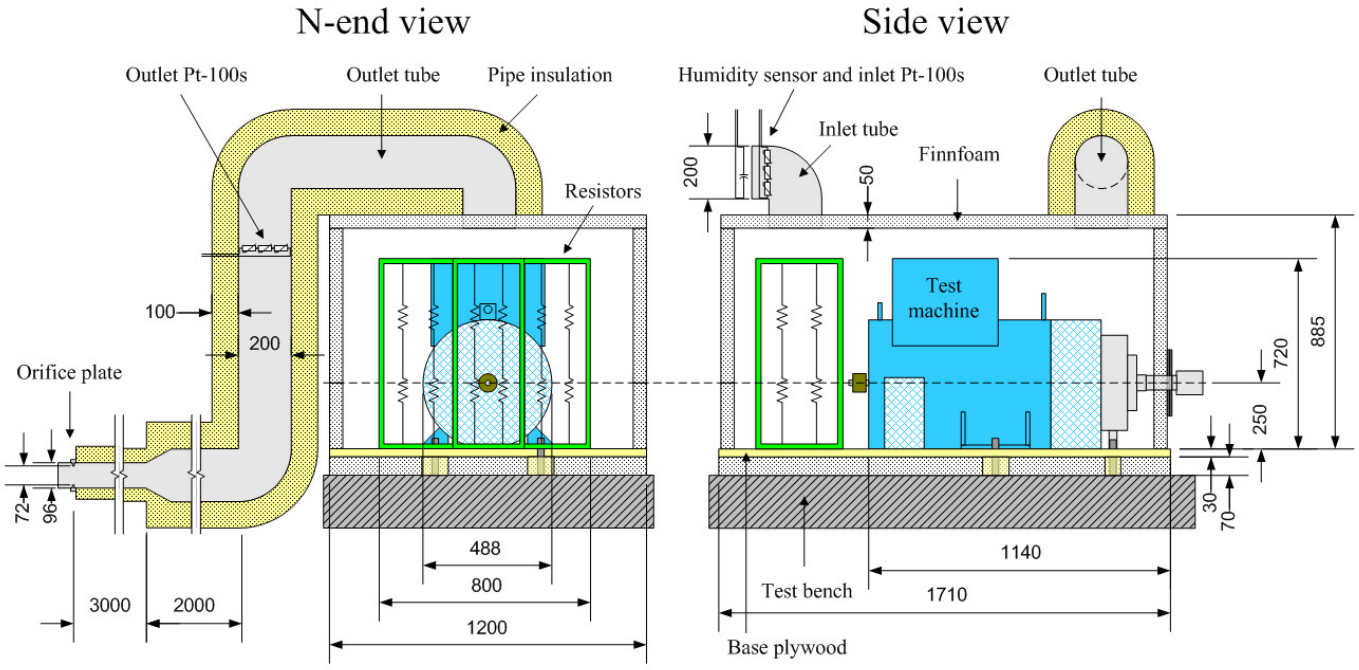

Fig. 2 Dimensions (mm) of the setup and placement of the temperature, humidity and mass-flow measurements.

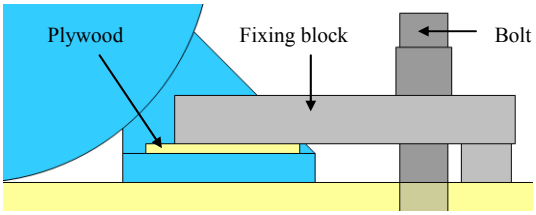

a)

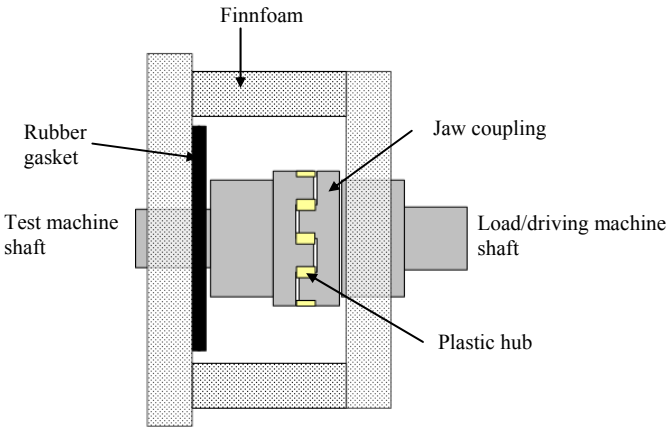

b)

Fig. 3 Insulation of a) the mounting and b) the shaft hole and the coupling,

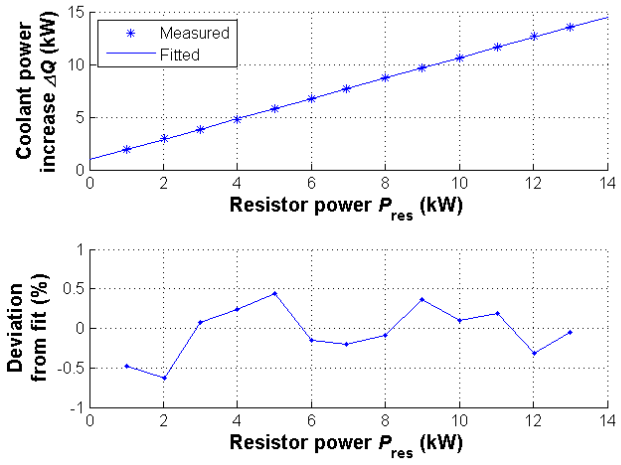

Fig. 4 Measured thermal power increase vs. calibration power and deviation of the measured points from the fitted line.

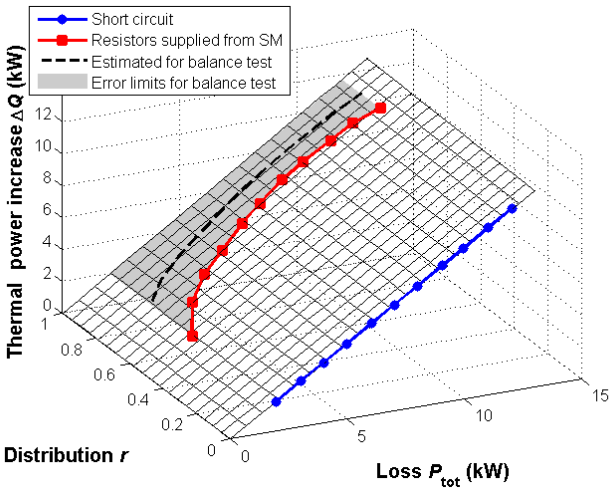

Fig. 5 Determination of the leakage difference between the balance test and short-circuit test.

TABLE I

METHODS AND ERRORS OF MEASUREMENT

Measurement	**Sensor**	**Meter**	**Error**
Differential pressure Δp	50-mbar differential pressure transducer	Fluke Hydra 2625A + 2620A	±68.5 Pa
Absolute pressures p_{hi}, p_0	1-bar absolute pressure transducer	Fluke Hydra 2625A + 2620A	±2742 Pa
Coolant temperatures T_{in}, T_{out}	Pt-100 sensors, 4-wire measurement	Fluke 8842A	±0.2 °C
Relative humidity RH_{in}	Temperature-compensated capacitive humidity sensor	Fluke Hydra 2625A + 2620A	±3 %RH
Armature currents	300-A current shunts	LEM Norma D 6000	±0.24…0.29 %
Field-winding power	100-A current shunts and voltage sensing	LEM Norma D 6000	±0.31 %
Cooling curve of armature resistance	10-A current source, a current shunt and voltage sensing	Fluke 8842A	±0.42 %
Torque during calibration tests	200-Nm torque transducer	HBM MD 18 N torque amplifier	< 1 %

TABLE II

MEASURED THERMAL POWER INCREASE AND ELECTROMAGNETIC LOSSES AT DIFFERENT LOADS

Operating point	$(P_{in\text{-}out} \pm \Delta P_{in\text{-}out})/a_0$	$\Delta Q \pm \Delta(\Delta Q)$	$P_{em} \pm \Delta P_{em}$	$P_{Cu,s} \pm \Delta P_{Cu,s}$	$P_{Cu,r} \pm \Delta P_{Cu,r}$	$P_{core} \pm \Delta P_{core}$
No load (generating)	2311 W ± 299 W (13.0 %)	2518 W ±80 W (3.2 %)	1686 W ±84 W (5.0 %)	0	147 W ±0.5 W (0.31 %)	1539 W ±84 W (5.5 %)
Half load (motoring)	4847 W ± 307 W (6.3 %)	4791 W ±114 W (2.4 %)	4097 W ±119 W (2.9 %)	1181 W ±7.8 W (0.66 %)	703 W ±2.2 W (0.31 %)	2213 W ±119 W (5.4 %)
Rated load (motoring)	11308 W ± 328 W (2.9 %)	11223 W ±201 W (1.8 %)	10908 W ±211 W (1.9 %)	5702 W ±40 W (0.71 %)	2267 W ±7.0 W (0.31 %)	2939 W ±215 W (7.3 %)